THE EFFECTS OF TOWFISH MOTION ON SIDESCAN SONAR IMAGES: EXTENSION TO A MULTIPLE-BEAM DEVICE

S.D. ANSTEE

MRL-TN-660

FEBRUARY 1994

MATERIALS RESEARCH LABORATORY
DSTO

The Effects of Towfish Motion on Sidescan Sonar Images: Extension to a Multiple-Beam Device

S.D. Anstee

MRL Technical Note
MRL-TN-660

Abstract

A simulation algorithm previously used to estimate the geometrical effects of towfish motion on single-beam sidescan sonar images is modified to simulate a multiple-beam sidescan sonar. The parameters of the sidescan sonar model are based on those announced for the Multiscan sonar soon to be manufactured by Klein Associates Inc. The results of simulations using the algorithm are discussed and compared with previous results for a single-beam device. The thresholds for towfish motions producing unacceptable image distortion are found to be similar to those found for the single-beam device. The image distortions induced by the motions are however found to be qualitatively different from those seen with the single-beam sonar. The effects of and limitations to a simple yaw-correction scheme are also discussed.

DEPARTMENT OF DEFENCE
DSTO MATERIALS RESEARCH LABORATORY

Published by

DSTO Materials Research Laboratory
Cordite Avenue, Maribyrnong
Victoria, 3032 Australia

Telephone: (03) 246 8111
Fax: (03) 246 8999

AR No. 008-628

APPROVED FOR PUBLIC RELEASE

Contents

The Effects of Towfish Motion on Sidescan Sonar Images: Extension to a Multiple-Beam Device

1. Introduction

Multiple-beam sidescan sonars are currently being developed by a number of manufacturers. Due to the faster coverage and increased resolution they offer in comparison to single-beam sidescan sonars, such devices are under consideration for acquisition by Navies requiring a minesweeping and route-survey capability.

A previous report (Anstee, 1993), hereafter referred to as Report **I**, discussed the effects of towfish (transducer) motions on the images from a single-beam sidescan sonar, established approximate limits for acceptable motions and indicated the qualitative effects on the sidescan image which could be expected from such motions. The purpose of this report is to examine a typical multiple-beam sidescan sonar using the same criteria that were used for the single-beam sonar, and to compare the results of single and multiple-beam simulations.

Theoretical and practical aspects of multiple-beam sidescan sonar manufacture have been discussed by Fox (Fox and Denbigh, 1983, Fox, 1985), who built a sidescan sonar capable of forming 5 beams simultaneously, for his PhD thesis. Subsequent to Fox's work, Klein Associates Inc. introduced a prototype multiple-beam sidescan sonar, also a 5-beam device. The sonar was evaluated during extensive TTCP Panel GTP-13 sea-trials in Bigbury Bay, UK and beam profiles for the device were also measured using the RDV Crystal facility in the UK (Huff *et al*, 1991). In work following the TTCP trials, (Huff and Weintroub, 1992, Huff, 1993) it was shown that the prototype sidescan sonar was capable of resolving targets with a performance matching theoretical expectations based on the specifications of the device, and Klein Associates continued to develop the sonar. A production version, the Multiscan sonar, will be available in 1994 and will be acquired by the RAN for evaluation purposes. In this report some of the parameters publicly announced by Klein Associates for the Multiscan sonar are adopted in the sidescan sonar model, which is referred to as the "MBEAM" sonar model.

In particular, parameters adopted for the MBEAM sonar model which are common to those announced for the Multiscan sonar are:

1. the operating frequency is 390 kHz;
2. the number of beams formed simultaneously on reception of each pulse is five;
3. individual transducer elements in the transducer packages are 100 mm long.

The operation of a multiple-beam sidescan sonar is similar to the operation of a single-beam device. Linear transducer packages are located on both sides of a towfish, which is towed behind a ship on a cable and forms beams perpendicular to the along-track (towing) direction, which are very narrow along-track. The multiple-beam device is more sophisticated than a single-beam device and uses dynamic focussing and steering techniques to form simultaneously several beams which are parallel to each other and equally spaced along-track. Array-shading techniques are used to keep the widths of the beams approximately constant and equal across most of the swath of the sonar. Simultaneous beam formation gives the option of increased resolution, greater towing velocity, or both.

The MBEAM model sonar forms five simultaneous beams from each ping. Depending on the range-scale required (that is, the distance from the tow track to the edge of the swath) the towing velocity is adjusted to keep the beam-to-beam distance constant along-track. This requires the towfish to move five times the distance between beam centres, between each pulse. For example, a typical towing velocity for the sonar is 9 knots with a range scale of 100 m, twice what could be expected from a single-beam device at the same range scale. This would allow beam centre separation of 12 cm, as opposed to 30 cm for the single-beam device.

In order to estimate the effects of towfish motions, a numerical model developed for a general single-beam sidescan sonar (Report I) was adapted to model a selected configuration of the MBEAM sonar. The model allowed the simulation of sidescan sonar images during different towfish motions. Most of the simulations involved minelike objects. The towfish motions which were modelled were generally identical to those used in the single-beam study, in order to allow direct comparisons between the results. Some representative examples from the simulations are included in this report.

It is was found from the modelling reported here and in Report I that the sidescan image is more sensitive to yaw than any other motion. The dynamic nature of the beamformers makes possible some degree of correction for towfish motions. The generic multi-beam model was extended slightly to allow for a simple form of yaw-correction, and this was sufficient to reveal both benefits from, and limitations to such a system. Examples of this are presented in Section 7.

Reference is made throughout this report to Report I, which should be read in conjunction with this report. Definitions for most of the terms used here are contained in the text and glossary of terms in Report I. Figures from Report I are also referenced in this report.

2. *The Multiple-Beam Sidescan Model*

The algorithm used in this work is an adaptation of the single-beam algorithm, and retains most of the approximations used there. The coordinate systems used in the single-beam case are retained, and the same symbols are used where possible. Refer to Report I for the single-beam system definitions.

2.1 The Towfish

The towfish is similar to the device described in Report I, although it is larger and heavier. As before, a local coordinate system attached to the towfish is used, shown in Figure 1, with the nose pointing along the positive z-direction, the *x*-direction pointing to port and the *y*-direction pointing to the top of the towfish. Note that the local coordinate system is denoted by lower-case letters (*x,y,z*) in contrast to the "world" coordinate system (*X,Y,Z*), which is attached to a point on the bottom. The transducer packages are aligned parallel to the z-axis, symmetrically on either side of the towfish. It is assumed that the centre of mass is at the origin of the local coordinate system, and that the transducer packages are symmetrical about the y-z plane.

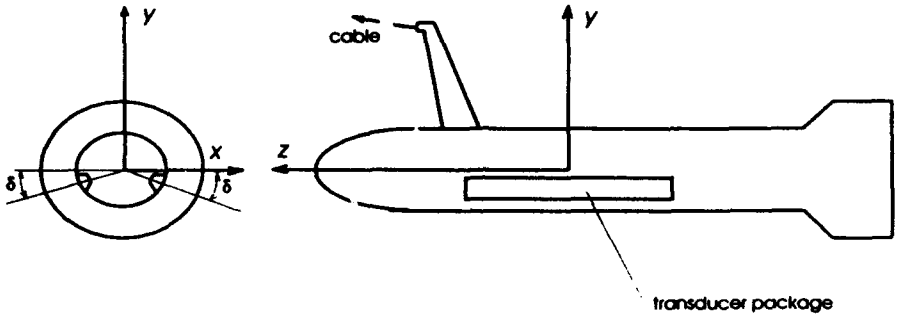

Figure 1. *Front cross-section (left) and side view (right) (not to scale) of a sonar towfish showing the local coordinate system with its origin at the nominal centre of mass. The towfish moves in the positive z-direction. The x-direction is positive to port. The transducers are tilted downward from the horizontal by a depression angle* δ.

2.2 Transducers

The transducer packages each contain a line of separate small, unfocussed linear elements laid end to end with little separation between them. Each element is connected to the beamformer separately, allowing focussing and steering by phase-shifting and weighting of the elements. The MBEAM sonar model assumes that enough elements are present to allow dynamic focussing and steering of the beams across the entire sidescan swath.

The same transducers are used for emission and reception, although the emission and reception beams have different forms, and different element weights are used to produce the beams.

2.2.1 *Beam Profiles*

The multi-beam sonar uses different beamforming at pulse emission and reception in order to maintain adequate coverage of the sea floor. Both sets of beams are relatively narrow along-track and broad across-track, but the beam at emission is broader along-track than the beams on reception.

The object of the beam formation at emission is to provide an adequate coverage of the sea floor for subsequent multiple parallel beam formation during reception. For this to occur, a rectangle on the bottom must be ensonified, wide enough to allow 5 beams to be formed on reception.

In order to achieve this, the MBEAM model assumes that the technique described by Fox (1985) is used, that is, the beamformer emits a toneburst, which is broken into five equal time sections. Each section of the toneburst is then emitted by a single transducer element, chosen for its proximity to the z-value of one of the beams formed at reception. Because the toneburst is staggered at emission, the sections of the toneburst cannot interfere with each other sufficiently to produce a focussed beam or an interference pattern. Thus, the beam at emission is approximately the sum of 5 independent beams, each radiating from a single transducer. The along-track beamwidth of each of the beams is approximately 2°, given an individual element length of 100 mm and an operating frequency of 390 kHz.

Rolling motions were found to have little impact on sidescan images in Report I, so they are not considered in this work, and the across-track variation of the beam pattern is neglected. Thus, expressions for linear apertures are used both for emission and reception beam pattern calculations in this work.

Beam formation during echo reception is intended to produce five parallel, equal width uniform beam patterns on the sea floor. This is achieved by multiplexing the responses of each of the transducer elements and sending them simultaneously to five dynamic beamformers. The beamformers adjust phase-shifts and element weights as a function of the echo return time. The phase-shift adjustments steer the beams continuously in order to maintain the centre of each beam at a constant distance along-track. The element weight adjustments effectively change the length of the array in order to keep the beamwidth constant across the swath.

It is assumed in the MBEAM model that (during reception):

1. Phase and element weight adjustments are made so frequently that changes appear to be continuous;
2. The transducer elements are small enough for the effective array length adjustment made by element weighting to appear continuous;
3. The same beam profile applies to each of the five beams, and this profile is maintained at all slant ranges;
4. The profile of each beam is that for a focussed, uniformly-weighted linear aperture whose centre is at the centre of the beam. That is, the profiles of all the beams are the same at the same range.

In practice, the beam formation is a complicated function of the (staggered) toneburst signal, the phase and element weighting values and update frequency, the electrical and medium errors in the system and the limitations of the array. In order to avoid unnecessary complication, the simplest models of the emission and reception beam patterns are used.

At emission, it is assumed that the staggered portions of the toneburst result in independent beams which can be simply added, since the echo from the entire toneburst is recorded on reception. Let the central beam be located in the *towfish*-coordinate x-y plane, and let the centres of the other beams be separated by a constant z-offset ξ, which will be the separation of the beams formed on reception. Thus, the beams are located in planes (relative to the towfish coordinate system)

$$z_0 = 0, \pm\xi, \pm 2\xi$$

It is assumed that each individual transducer element can be approximated by a linear aperture of length d. Assume that the transducer elements are centred in the same planes as the beam centres. It is convenient to take the world coordinate (X',Y',Z') of a point on the bottom and transform it the point (x',y',z') in the towfish coordinate-frame, in the same manner as was discussed in Section 3 of Report I. Then the energy beam pattern *at emission* can be estimated by the sum of the beams from each of the transducers impinging on the point, one after the other, given by

$$b_e(z',r')$$
$$\equiv b_1(z'-2\xi,r')+b_1(z'-\xi,r')+b_1(z',r')+b_1(z'+\xi,r')+b_1(z'+2\xi,r')$$

where $b_1(z)$ is the directivity function of a single linear aperture and is given by

$$b_1(z) = \mathrm{sinc}^2\left(\frac{dv}{\lambda}\right)$$

where $v = z/r$ and r is the slant range to the point (normally estimated by the distance from the point to the centre of the array). Note that close to the array, a point on the bottom may only be ensonified significantly by one of the transducers, while a point further from the towfish might be ensonified by all of them.

For the beam patterns at reception, the assumptions mentioned previously hold, so that each beamforming mechanism can produce a beam of fixed -3 dB beam width w_{3dB} centred about an arbitrary z-plane, which is uniform at all ranges across the entire swath. Assuming that the beamforming was achieved by adjusting the effective length of the array to obtain the desired beamwidth, then the expression for the beam pattern can be approximated by the beam pattern of an unshaded linear aperture. The fact that the array is focussed at all ranges means that the far-field expression for the beam pattern can be used at all ranges. The assumption that the centre of the beam along-track coincides with the centre of the effective extent of the array means that the beam profile is symmetric about the centre of the beam. In addition, since the width of the ensonified patch on the sea bottom created by the emission beams is always much smaller than the slant range, the curvature of the reception beam pattern can be neglected. We can approximate the far-field beam pattern expression by

$$b_r(z,z_0,r) \equiv \mathrm{sinc}^2\left(\frac{L_{\mathrm{eff}}(z-z_0)}{\lambda r}\right) = \mathrm{sinc}^2\left(\frac{0.88(z-z_0)}{w_{3dB}}\right)$$

where z_0 is the location of the centre of the beam along-track, given by one of the five values noted above, L_{eff} is the effective length of the array and the -3 dB width of the beam pattern is related to the effective array length by

$$w_{3dB} \cong 0.88 \frac{\lambda r}{L_{eff}}.$$

For the current modelling, we choose beamwidths of 200 and 300 mm for the MBEAM sonar. As noted in Report I, given that geometrical effects due to towfish motion are of primary interest in this work, the treatment of the beam patterns above should be adequate.

2.3 *The Sea Floor, Targets and Propagation*

The properties of the sea floor, targets and propagation are all assumed to be the same as for the single-beam calculations of Report I, and are described there in Section 2.3.

2.4 *The Sidescan Image*

The MBEAM sonar produces an image very similar to that of a single-beam device, except that five stripes (or a subset of them) are put on the image after each pulse. Similarly to the single-beam case, a Time-Varying Gain (TVG) function is used to maintain a uniform background level across the swath. However for the MBEAM sonar a different TVG function is required for each of the five beams. This is because:

1. The emission beam pattern b_e peaks in the centre at $z = 0$ where the overlap of all 5 beams is greatest, and;
2. Towfish motion between pulse emission and echo reception also has an effect.

As described in Report I, the TVG function is assumed to compensate perfectly for across-track variations in the background level of the image. Again, an artificial TVG function is calculated to normalise the simulated sidescan image, using stable motion above an evenly reflective bottom.

3. *Treatment of Towfish Motion*

The model described in Section 3 of Report I applies without modification to this work. All the symbols and notations used there are retained in this work.

4. *The Sidescan Simulation Model*

An adaptation of the iterated method from Report I was used for image simulation. Only differences from Section 4 of Report I are reported here. The three-stage calculation is retained, as is the representation of the bottom via reflectivity of a grid of rectangles. An additional constraint is that V_0, the towing velocity, is related to the separation between beam centres ξ, by $V_0 = 5\xi/T$, where

T is the time separation between pulses. (Or it is assumed that the ship's tow speed will be adjusted such that this condition is satisfied.)

The first step of the simulation now yields an "energy" incident on the ijth rectangle from the nth pulse, of

$$E^I_{ijn} = b_e\left(\left[\mathbf{q}'_{ij}(t)\right]_z\right)$$

retaining the notation of Report I, except that $[\ ]_z$ refers to the z-value of the point in the local towfish frame. Note that i is the index in the x-direction, and j is the index in the z-direction. $\mathbf{q}'_{ij}(t)$ is the position of the central point of the ijth rectangle on the bottom, relative to the towfish coordinate frame.

The second step of the simulation is complicated by the fact that for each pulse n, five beams are formed. Let the beams be known as $\beta = 1, 2, \ldots 5$, increasing along-track. Then the "energy" response induced in the βth beamformer from an echo from the ijth rectangle and the nth pulse has the relative value

$$E^R_{ijn\beta} = \rho_{ij} b_r\left(\left[\mathbf{T}\left(t'_{ijn}\right)\left\{\mathbf{q}_{ij} - \mathbf{p}\left(t'_{ijn}\right)\right\}\right]_z, (\beta-3)\xi\right) E^I_{ijn}$$

where the notation of Report I has been retained, that is, ρ_{ij} is the reflectivity of the ijth rectangle, $\mathbf{T}\left(t'_{ijn}\right)$ is transformation matrix from the world to local towfish coordinate frame at the moment of return t'_{ijn} of the echo from the ijth rectangle from the nth pulse, $\mathbf{q}_{ij}$ is the position of the centre of the ijth rectangle in the world coordinate frame and $\mathbf{p}\left(t'_{ijn}\right)$ is the position of the towfish in the world coordinate frame at the moment of return of the echo.

For the third step of the simulation, the raw simulated sidescan image is formed from pixels $G_{k\beta}$ which are the sum of energies $E^R_{ijn\beta}$, assigned to the nearest range-bin k as noted in Report I.

Finally, normalisation values for the raw sidescan image, say $G_{k0\beta}$, pre-calculated from a single pulse and an evenly reflective bottom $\rho_{ij} = 1$ for stable motion at constant velocity V_0, are applied to (divided into) the $G_{k\beta}$ and the simulated sidescan image is ready to display. Maximal energy values E^I_{ij} and E^R_{ij} for each rectangle are also recorded, similarly to the cases in Report I, where the maximum now applies over all pulses n and beams β. Again these show incident and received beam footprint patterns on the bottom. Examples of these were presented in Report I.

5. *Measures of Distortion*

5.1 Local Measures of Distortion

The analytically calculated "measures" given in Report I to estimate distortion thresholds are not appropriate without some modification for the multiple-beam case, and in fact may not be very useful given the differing nature of the system. Because multiple beams are formed simultaneously, the pulse-to-pulse estimates

for the single-beam sonar should apply directly only to the last beam formed in one pulse and the first beam formed in a successive pulse (say, the "beam-to-beam" distortion). However the effects on the central beams from successive pulses also provide an estimate of the distortion of the image considered as a whole (say, the "pulse-to-pulse" distortion). The gross effects on the image will also be different in the multiple-beam case, since beams from the same pulse remain parallel regardless of towfish motions. This can allow the duplication of entire objects, which could be a serious problem if small objects (for example, mines) are important in the image.

5.1.1 *Backscanning*

The minimum along-track separation between pulses δZ given as a criterion for backscanning in Report I becomes, on a neighbouring-beam basis,

$$\delta Z = \xi - A\sqrt{2 - 2\cos(\omega T_p)}$$

where ξ is the separation between beam centres, while on a neighbouring-pulse basis it retains the form given in Report I. Since in general the beam separation ξ is smaller than the equivalent quantity for a single-beam sonar ($l_0 T_p$ in Report I), this suggests that the multiple-beam device may be more sensitive to surge, pitch and yaw motions than the single-beam device. However, considering successive pulses, the quantity $l_0 T_p$ for the multiple-beam sonar may be larger than that for a single-beam device, indicating reduced sensitivity to the same motions. This is discussed later in the report, using the results of sidescan simulations.

5.1.2 *Average Magnification*

The "fractional distortion" measure given in Report I suffers from the same ambiguity as the backscanning measure. We have

$$\frac{\langle \delta \rangle}{\Xi} = \frac{A\sqrt{1 - \cos \omega T_p}}{\Xi},$$

where Ξ is ξ for a beam-to-beam calculation and $l_0 T_p$ for a successive-pulse calculation, indicating effects differing by a factor equal to the number of simultaneously-formed beams.

5.2 *The Probability of Non-Detection of an Object*

The same algorithm given in Report I for the probability of non-detection of an object also applies to the multiple-beam results, since the maximal energy values E_y^R are produced by both simulation methods.

6. *Results from Numerical Simulations*

Numerical simulations for most of the towfish motions studied in Report I were repeated using the MBEAM sonar model given in this work, in order to provide a most meaningful comparison. Comparisons were made between the MBEAM results and the 380 kHz single-beam results, rather than the lower resolution 108 kHz option of the single-beam sonar.

The simulations used the "target" sea floor model described in Report I, that is, arrays of minelike objects on a completely unreflective sea floor. The "blank" sea floor was not used, since it was noted in the previous work on the single-beam sonar that the distortion induced by the towfish motions was more important than the effects of degraded bottom coverage due to the same motions.

6.1 *Operating Settings*

In the absence of a standard setting, the simulations were made assuming the following conditions:

1. towing velocity 9 knots;
2. range scale 100 m, giving interval between pulses 0.13 s and separation between beams 120 mm;
3. altitude 10 m;
4. -3 dB beam width 200 mm.

Grey-scaled images were normalised as noted in Report I.

Sinusoidal motions were simulated with the starting phase set to zero.

Each simulation comprised a record of approximately 111 pulses, and consequently 555 beam returns. The area of the bottom represented in the simulations is the same as for the single-beam simulations.

Only examples of the results of the third stage of the simulations, the simulated sidescan images, are shown in this work.

6.2 *Simulations for Stable Motion*

Figure 2 shows the simulated sidescan image of the targets for stable motion at 9 knots. Comparing this with Figure 10 from Report I, the resolution of the MBEAM sidescan image is better than that of the single-beam image, due to the closer spacing between beams of the MBEAM sonar, but the difference is not large. The identical MBEAM simulation with 300 mm beamwidth showed the expected small decrease in resolution as compared to the result with the 200 mm beamwidth, but again the effect was not of large magnitude. Both MBEAM simulations showed a "halo" around the objects which is due to reception-beam sidelobes. The magnitudes of the haloes show a slight increase with increasing range, despite the fact that the beam widths of the reception beams are identical across the track. This appears to be due to the spreading of the emission beam pattern, which allows reception beam sidelobes to register slightly more on the image at large across-track ranges.

Coverage of the sea floor was excellent for both beam widths, as would be expected in stable conditions.

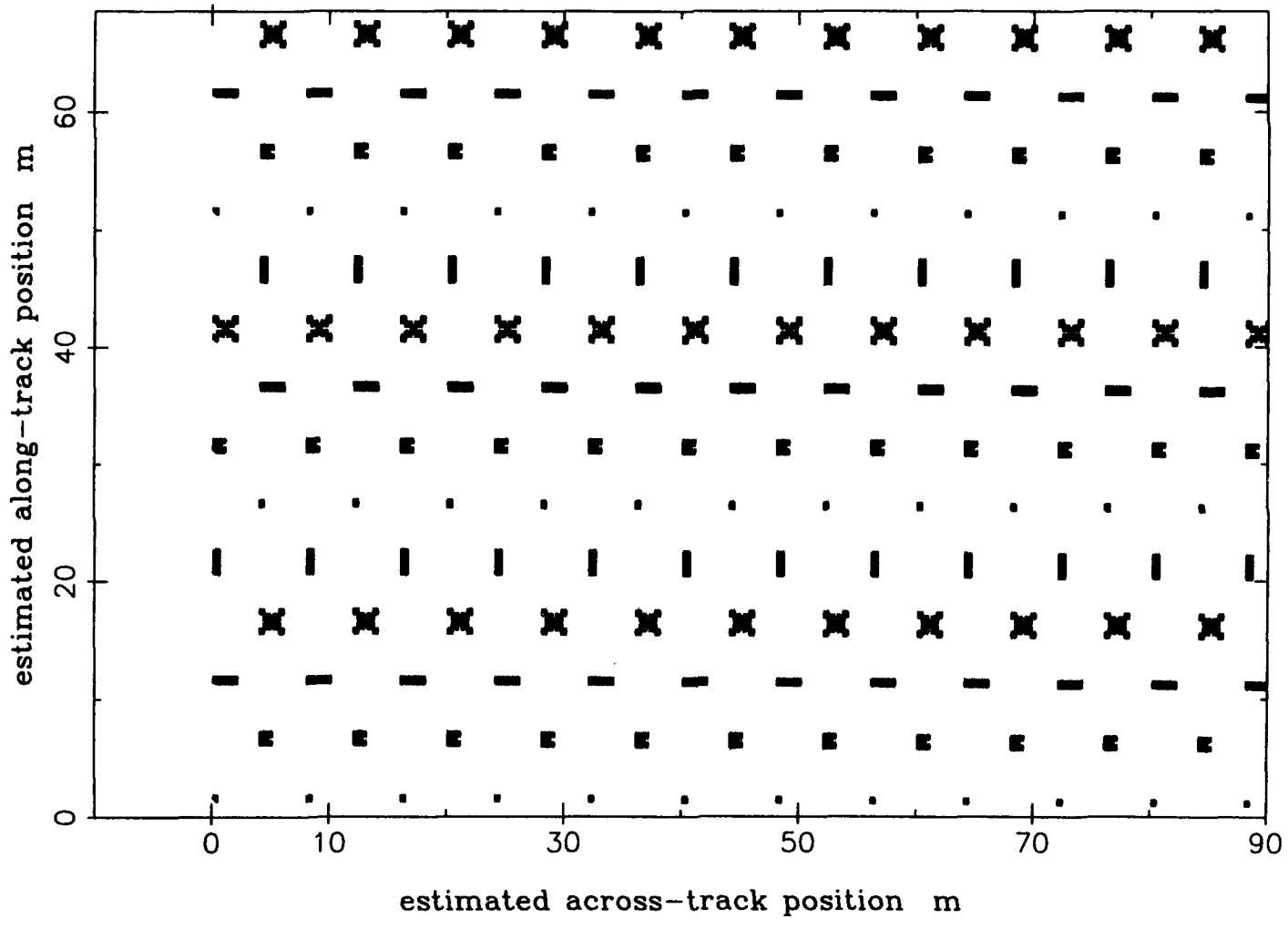

Figure 2: Simulated MBEAM image of the targets, for stable motion at 9 knots, altitude 10 m. Resolution is uniform across the swath, reflecting the uniform beam width of 200 mm. The "halos" around the images correspond to beam sidelobes.

The effects of differing values of towing velocity were not simulated. It is clear, however, that the MBEAM images will be sensitive to towing velocity, since the separation between neighbouring beam centres from successive pulses must be maintained equal to the separation between beam centres from the same pulse in order for the sidescan image to be geographically accurate. In conditions where a lower than ideal towing velocity was employed, software could be used to correct geographic distortions.

6.3 Some General Comments on the Simulations Including Towfish Motion

Comparisons of the MBEAM simulation results with those from the single-beam simulations of Report I, using the same towfish motions, revealed qualitative differences between the MBEAM and single-beam simulations.

The first qualitative difference between the MBEAM simulations and the single-beam simulations is that many of the MBEAM simulations appear coarser than the equivalent single-beam simulations. This effect results from the fact that five beams are formed simultaneously from each pulse and are subject to identical towfish motions. Thus, when a towfish motion results in pixel translation on the sidescan image, blocks of pixels corresponding to the five simultaneous beams appear translated, rather than the single stripes (rows of pixels) associated with the single-beam simulations. This effect makes the image appear coarser in many instances than the single-beam simulation (beam-to-beam distortion as defined in Section 5), but also has the effect of keeping images of objects which happen to fall within the beams from a single pulse, relatively undistorted. Thus, distortion relative to the single-beam case can increase in the region of a boundary between pixels corresponding to different pulses, while being decreased within pixels corresponding to the same pulse.

The second qualitative difference between the MBEAM and single-beam simulations reflects the particular parameters chosen for the MBEAM model. A towing velocity of 9 knots, twice that of the single-beam sonar, means that the MBEAM image considered as a whole, is less distorted than the equivalent single-beam image. Considering the "fractional magnification" expression in Section 5 on a pulse-to-pulse basis, it can be seen that the effect of the motion is inversely proportional to the towing velocity - in this case, the translation induced by towfish motion is effectively distributed over twice the distance along the bottom.

Given that beam-to-beam distortion, as defined in Section 5, is more severe in the MBEAM images than single-beam images, while pulse-to-pulse distortion is less severe, it should be appreciated that the estimates given below for limits on acceptable magnitudes of towfish motion depend on which type of distortion is most important to the viewer of the image.

The response of the simulations to a change in the period of the towfish motion is the same for the MBEAM model as it is for the single-beam model. In the MBEAM simulations, both the peak-to-peak and beam-to-beam distortions are inversely proportional to the period of the towfish motion.

6.4 *Simulations for Heave Motions*

Distortions observed in the MBEAM simulation images due to heave motions were similar in magnitude and extent to those observed in single-beam simulations.

Figure 3 shows the MBEAM simulation image of the targets for a 1 m heave with a period of 3 s. Comparing this with Figure 11 of Report I, there appears to be little significant difference, except that the groups of five rows of pixels are clearly visible at small ranges, and the slopes induced in the images of objects (considered as a whole) are smaller for the MBEAM image than the single-beam case. This is in line with the effects discussed in Section 6.3.

Approximately the same thresholds for heave amplitude which applied to the single-beam case also apply to the multiple-beam device. The threshold nominated in Report I was that heave amplitude should be less than 1/20th the smallest important across-track range, for altitude 10 m, and a period of 3 s.

If small objects, that is, with sizes of the order of twice the separation between beams, are of primary interest, then a smaller threshold may be appropriate for the motion, in line with a beam-to-beam separation of 120 mm in comparison to the single-beam figure of 300 mm, say 1/40th the smallest across-track range.

If larger objects are important, that is, objects with sizes larger than the pulse-to-pulse separation of 600 mm, then a larger threshold, say 1/10th the smallest important across-track range, may be appropriate for the limit on the heave amplitude.

6.5 *Simulations for Sway Motions*

Distortions due to sway are similar for MBEAM and single-beam simulations. Figure 4 shows the simulated MBEAM image of the targets during sway motion with 1 m amplitude and 3 s period. Comparing this image with Figure 12 of Report I, the obvious differences are again the coarseness of the MBEAM image and the reduction in overall distortion.

For small objects a limit of 0.5 m sway amplitude with a period of 3 s, the same as for the single-beam case, is appropriate.

For larger objects a limit of 1 m sway amplitude with a period of 3 s is appropriate.

As for the single-beam case the distortion caused by heave motion is easily corrected before display.

6.6 *Simulations for Roll Motions*

Simulations were not performed for roll motions. The conclusions that were reached in Report I for the single-beam sonar will also apply to the MBEAM sonar, since it is expected that the two devices will have similar across-track beam profiles.

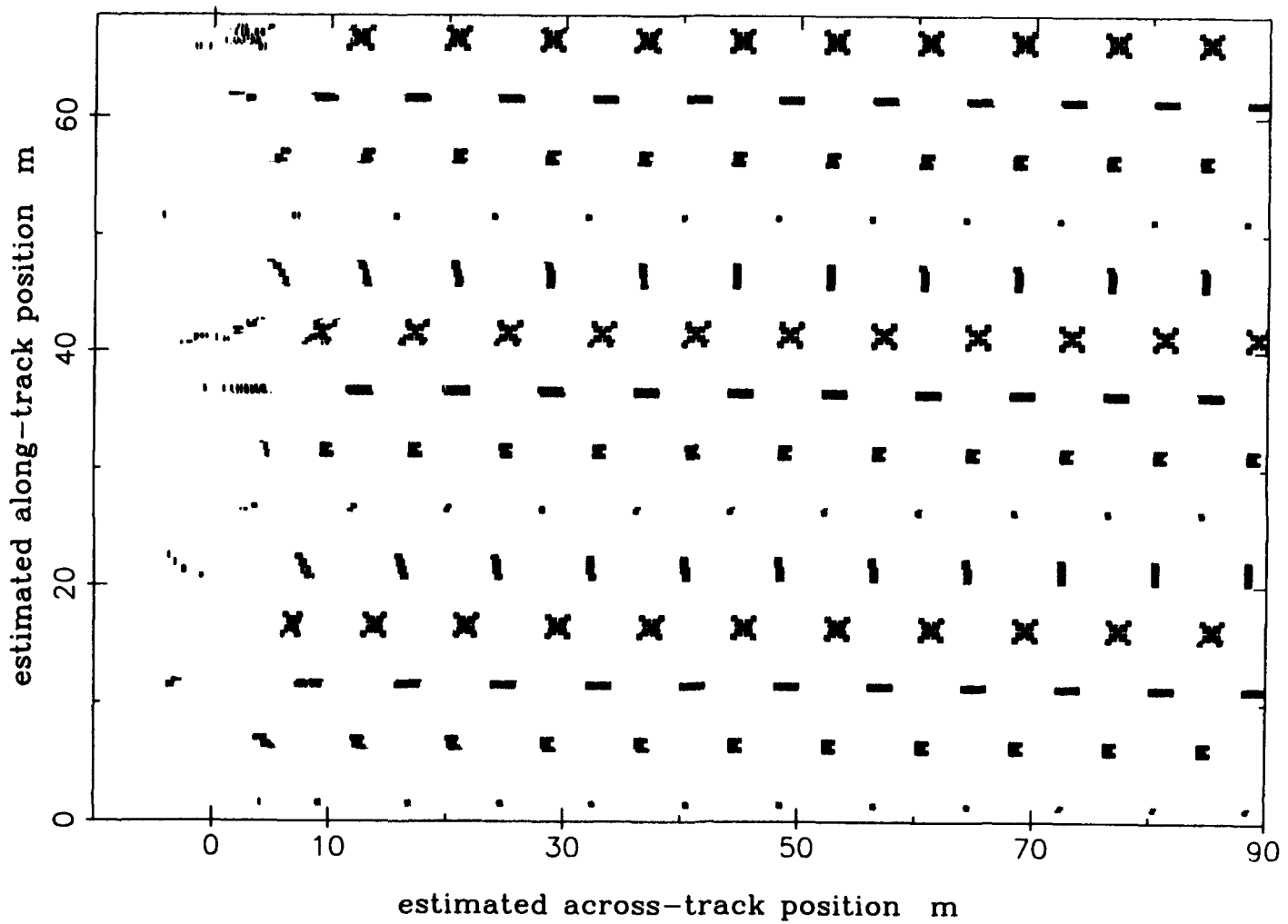

Figure 3: *Simulated MBEAM image of the targets, for a 1 m amplitude heave motion, period 3 s, about a towfish altitude of 10 m.*

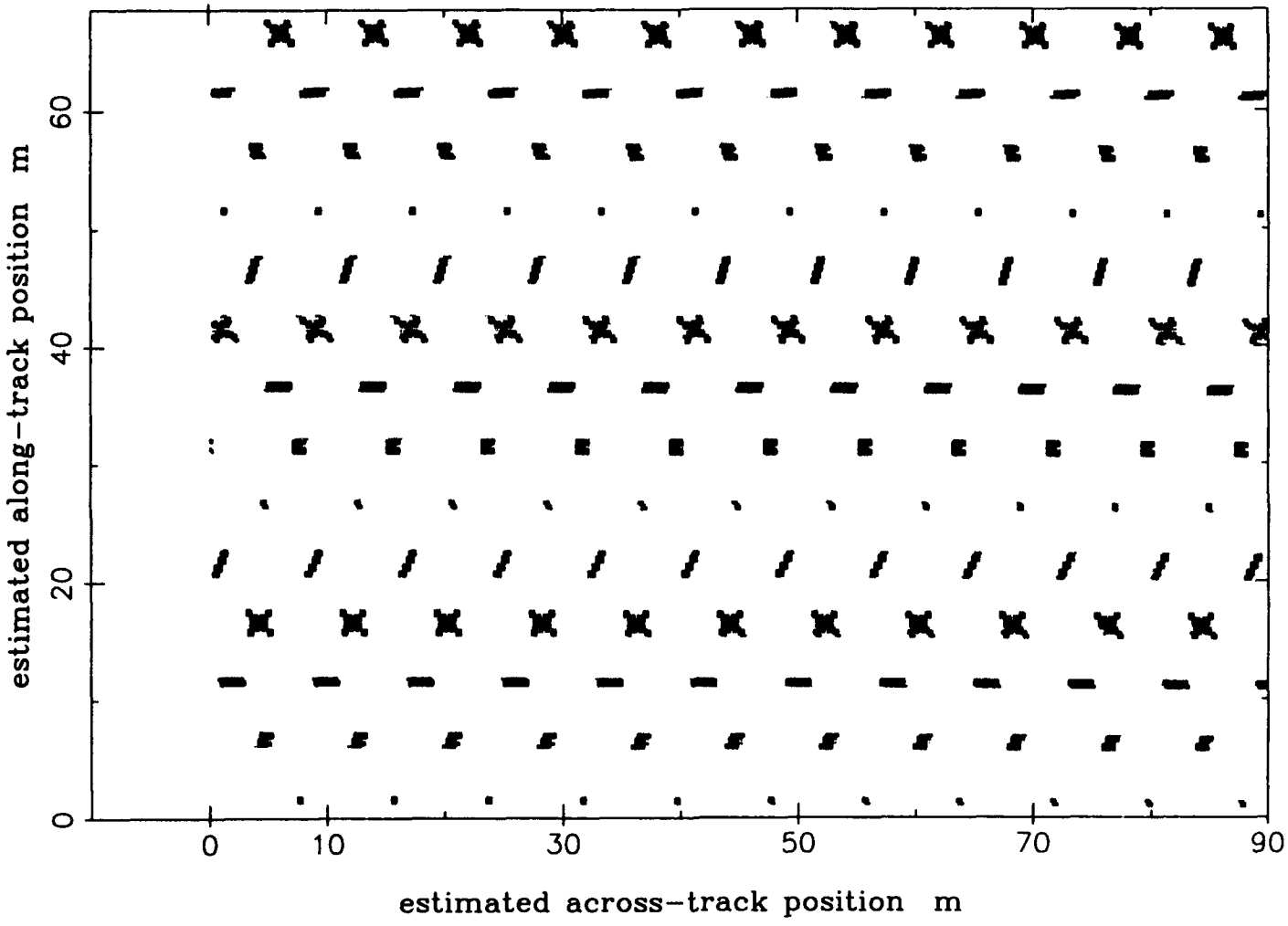

Figure 4: *Simulated MBEAM image of the targets, for a 1 m amplitude sway motion, period 3 s, towfish altitude 10 m.*

6.7 *Simulations for Pitch and Surge Motions*

A comparison of MBEAM and single-beam simulations for pitch/surge motions using the same values of amplitude and period showed that the thresholds for different types of distortion varied between the two sonars.

Neglecting the appearance of backscanning in the image, the MBEAM image was less distorted overall than the equivalent single-beam image in every case, for reasons discussed in Section 6.3.

Figure 5 shows the MBEAM image for a pitch motion with 3° amplitude and 3 s period at 10 m altitude. In contrast, Figure 14 of Report I shows the single-beam sidescan sonar image for the same towfish motion. Objects considered as a whole are less distorted in the MBEAM image than in the single-beam image. Only local blurring of some objects is worse for the MBEAM image than the single-beam image.

In general, the distortion from magnification and translation of objects in an MBEAM image was half that caused by a motion of equal amplitude and period in a single-beam image. This is caused by the fact that the MBEAM towing velocity is twice that of the single-beam sonar.

Distortion due to backscanning appeared at lower motion amplitudes in the MBEAM simulations than in the single-beam simulations. This is because the beam-to-beam separation of the MBEAM sonar is set to 120 mm, as compared to 300 mm for the single-beam sonar. Considering the expression for the threshold of backscanning given in Section 5, this shows that backscanning should appear for an amplitude 2.5 times smaller for the MBEAM sonar than the single-beam sonar, given the same altitude and period. This would correspond to an amplitude of approximately 4° with period 3 s and altitude 10 m, extrapolating from the results of Report I, where backscanning commenced at an amplitude of approximately 9°. However, the backscanning in the MBEAM case would be restricted to the edges of groups of five stripes from the same pulse. This presumably accounts for the extra blurring seen in the MBEAM image of some objects for a pitch motion of 3° amplitude, period 3 s, altitude 10 m. At larger pitch amplitudes, overlaps of two or more beam separations become important.

Backscanning effects become more obvious for a pitch motion with 6° amplitude, period 3 s and 10 m altitude, appearing as blurring and replication of parts of the image. At 9° amplitude the effect is widespread and at 12° amplitude, the entire image is badly distorted. However, backscanning in multiple-beam images has a different character to backscanning in single-beam images. In single-beam images, backscanned objects are inverted and magnified or diminished. Duplicated objects are often separate features in the image and do not necessarily have any clear origin. However, in the MBEAM images, the magnification effect is less pronounced, and backscanned images appear as multiple replications, which can be connected in the image. In some cases, the nature of the original object is clear even after multiple replication, since the set of five stripes formed by each pulse retains its internal coherence, and can be large enough to image the object.

Figure 6 shows the MBEAM image of the targets for a 12° pitch with a period of 3 s and altitude 10 m. Backscanning effects appear as multiple replications of the targets. Comparing this with Figure 15 of Report I, it is clear that the character of the distortion is different in the MBEAM simulation.

Assuming that the appearance of backscanning and magnification in the image denotes the threshold of acceptable towfish motion, a maximum acceptable pitch threshold of 6° amplitude, period 3 s and altitude 10 m is adopted.

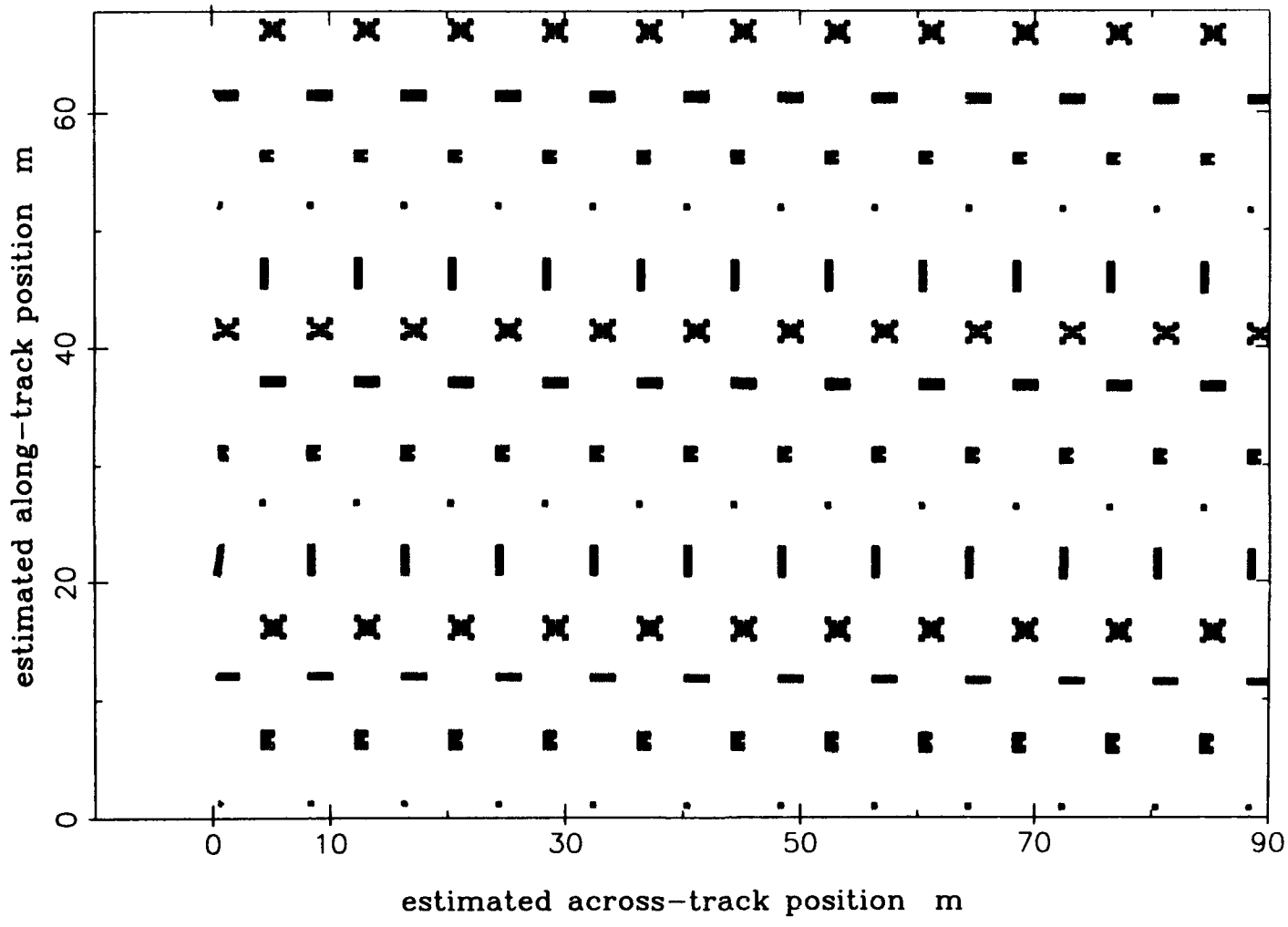

Figure 5: *Simulated MBEAM image of the targets, for a 3° amplitude pitch motion, period 3 s, towfish altitude 10 m.*

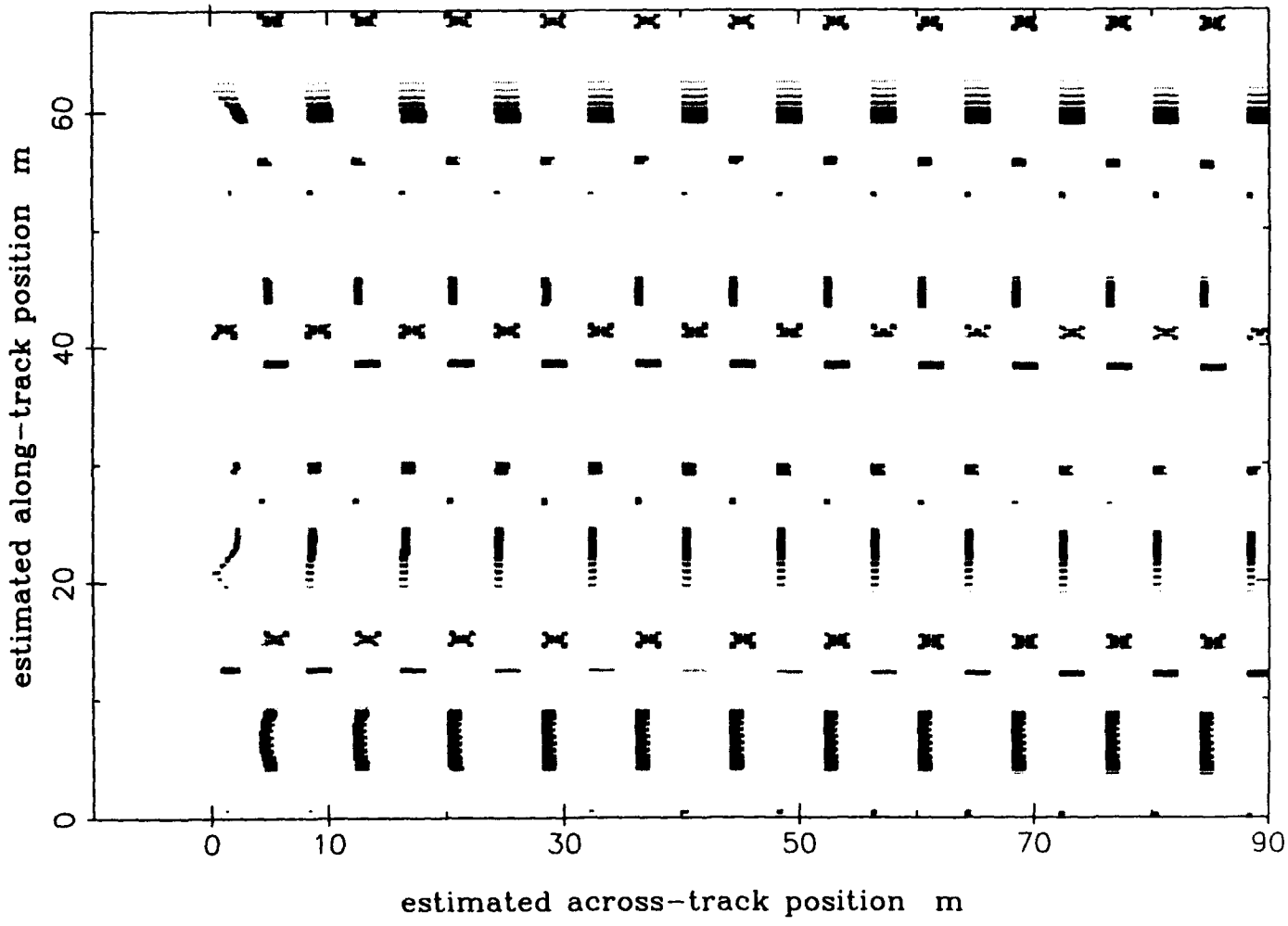

Figure 6: Simulated MBEAM image of the targets, for a 12° amplitude pitch motion, period 3 s, towfish altitude 10 m.

As noted in Report I, heave motion is approximately equivalent to pitch motion for small amplitudes, since both motions cause translations of the beams along-track. A 1 m amplitude heave motion is approximately equivalent to a 6° pitch motion with altitude 10 m. Heave amplitude then scales proportionally to pitch amplitude and towfish altitude, that is, the same pitch amplitude at twice the altitude is equivalent to double the heave amplitude and so on. The major difference between images from pitch and heave motions occurs close to the tow track, since pitch motions increase the distance from the towfish to the first bottom return, and induce an effect in the image similar to a small-amplitude heaving motion.

6.8 Simulations for Yaw

In Report I yaw motions were identified as having the most potential to damage single-beam sidescan images. This remains true for multiple-beam sidescan images, and the amplitudes identified as thresholds for damage of single-beam images are approximately correct for multiple-beam images.

The comments made in Sections 6.3 and 6.7 about the nature of distortions in MBEAM images remain pertinent to distortions induced by yaw, that is overall distortion is reduced at the cost of greater sensitivity to backscanning.

Figure 7 shows the MBEAM image of the targets with a yaw motion of 0.5° amplitude with a period of 3 s. Some distortion is evident in the image, however a comparison with Figure 16 of Report I shows that the MBEAM image is less distorted than the single-beam image. Figure 8 shows the MBEAM image for a 1° yaw amplitude with a period of 3 s. More distortion is evident, and backscanning has appeared at the outer edge of the image. Figure 9 shows the MBEAM image for a 2° yaw amplitude with a period of 3 s. Comparing this with Figure 17 of Report I, we see that both images are badly distorted for ranges above 30 m, however the character of distortion is very different. In the single-beam image, objects are duplicated and separated by backscanning, while in the multiple-beam image, objects are replicated more continuously. In general, the objects in the MBEAM image are more easily recognised, since the set of contiguous beams formed with each pulse is often enough to distinguish a particular object if it is of the order of the along-track distance covered by the beams. In the present case, the along-track distance imaged at each pulse is 0.6 m, and this could be increased up to 1.5 m if a 150 m range-scale setting were employed instead of the present 100 m, and the towing velocity were increased from 9 knots to 15 knots.

The simulations were not extended to amplitudes greater than 3°, period 3 s, since very severe distortions were seen in the 3° simulation, which were similar to the single-beam sonar case.

Considering the level of overall distortion in the images, a maximum value of 1° yaw, period 3 s, is tolerable in the MBEAM images, in contrast to the 0.5° limit of the single-beam sonar. However, where small objects are important and even limited backscanning cannot be tolerated, a maximum of 0.5° yaw, period 3 s, is more appropriate.

Distortion effects from yaw are expected to stay approximately constant, regardless of the range-scale chosen, since the beam translation along-track due to yaw is proportional to the horizontal range, but the beam centre separations are also proportional to the range scale (maximum range) chosen. Thus, the ratio of the yaw-induced beam translation to the beam centre separation should remain approximately constant.

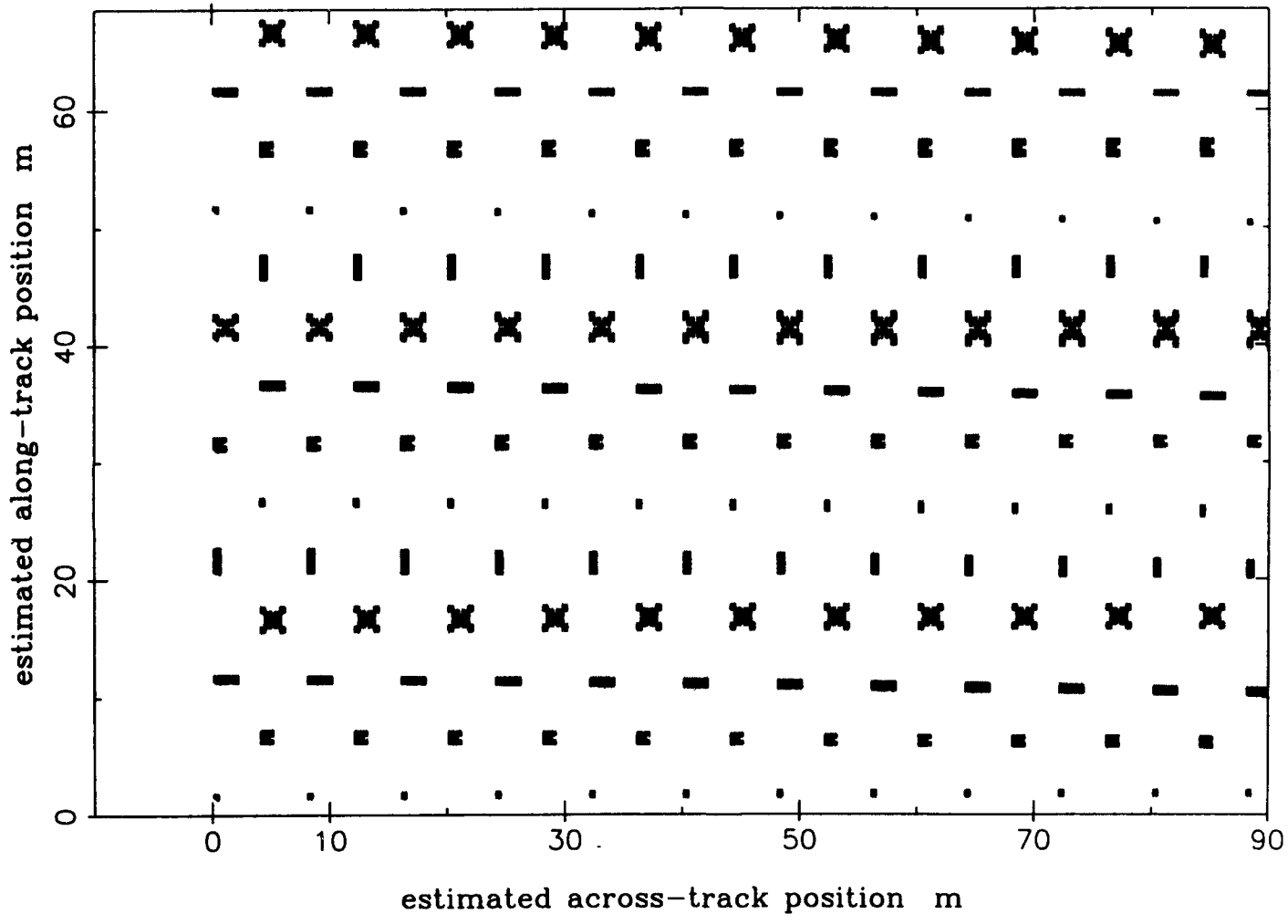

Figure 7: Simulated MBEAM image of the targets, for a 0.5° amplitude yaw motion, period 3 s, towfish altitude 10 m.

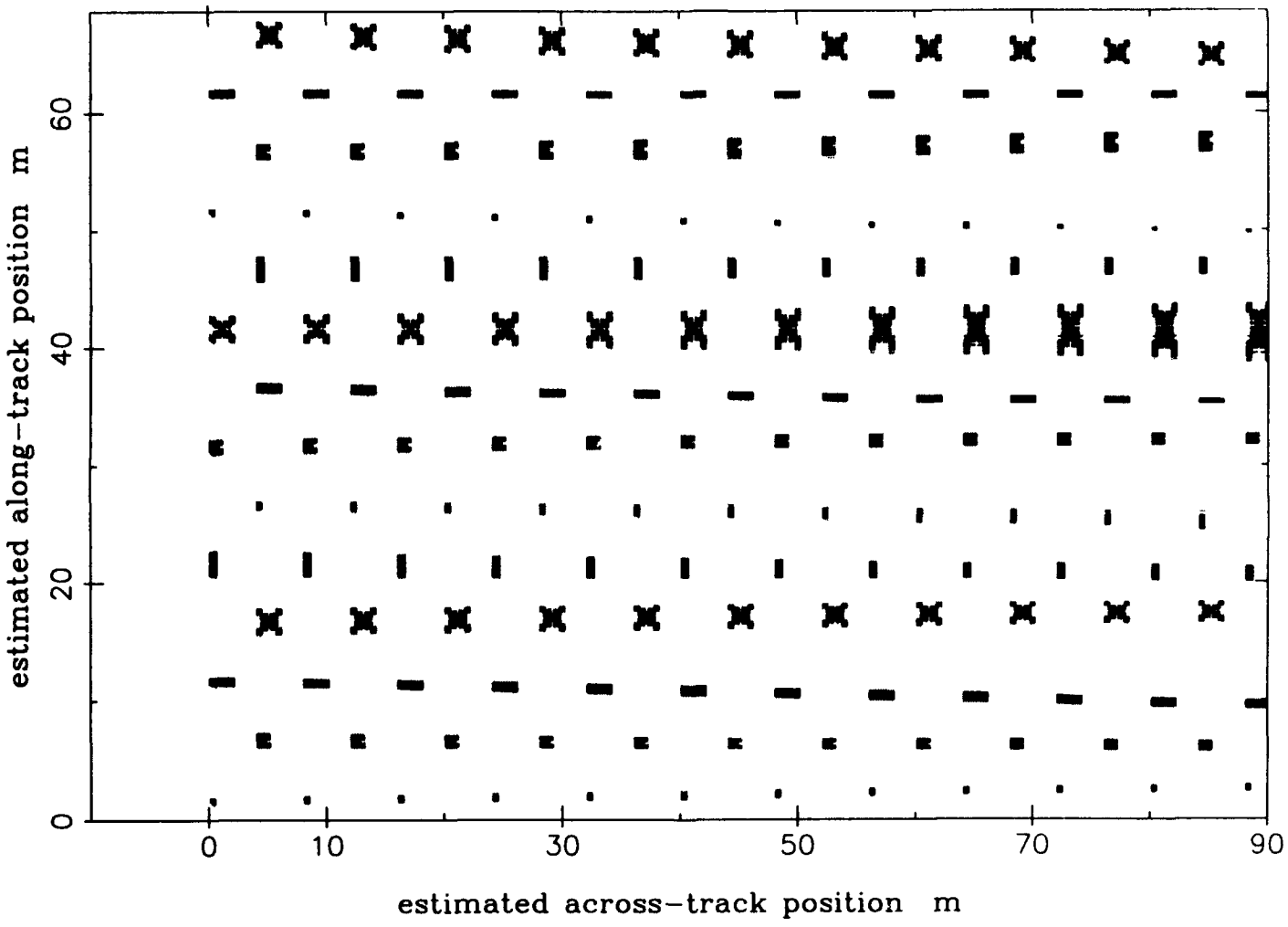

Figure 8: Simulated MBEAM image of the targets, for a 1° amplitude yaw motion, period 3 s, towfish altitude 10 m.

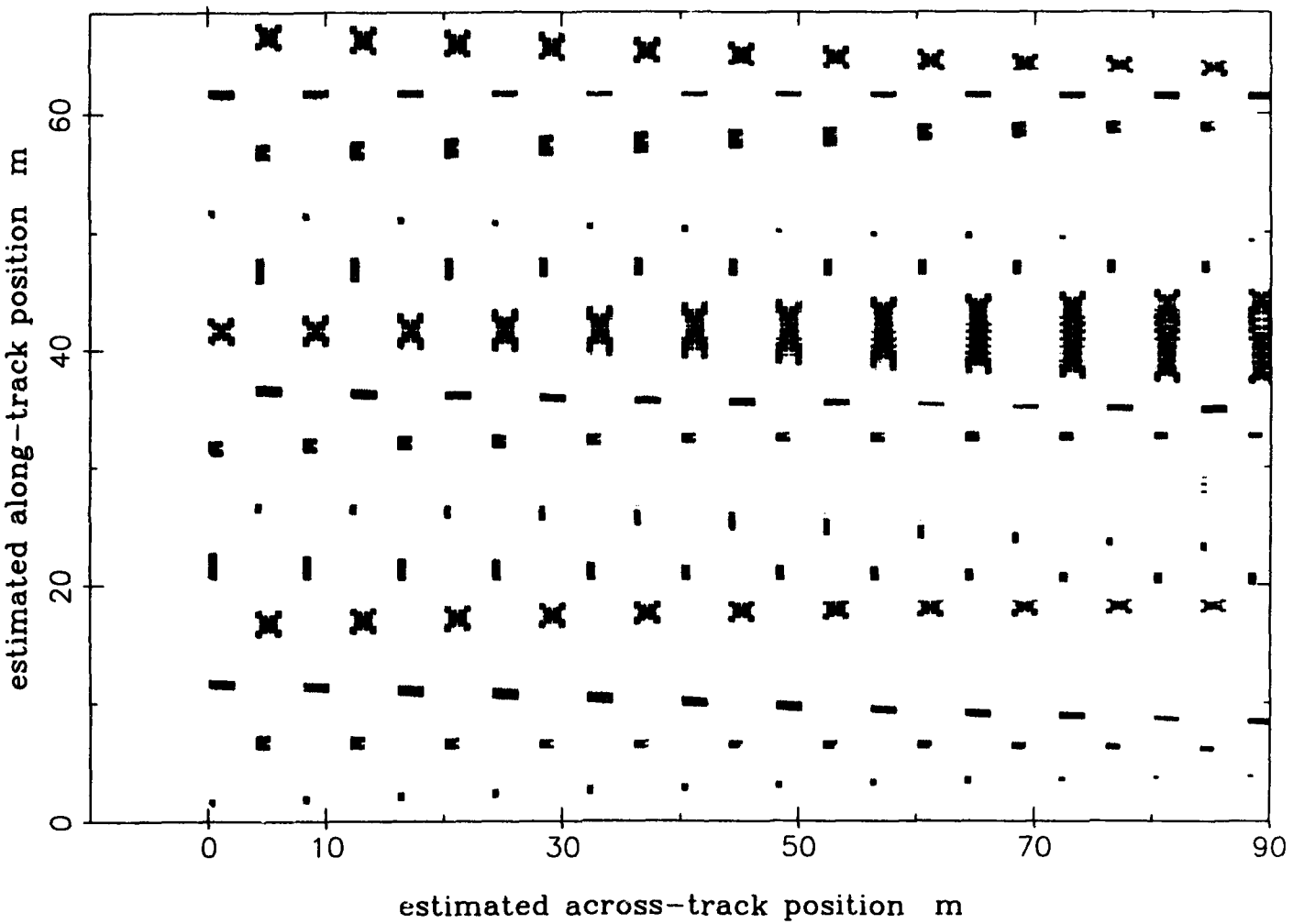

Figure 9: Simulated MBEAM image of the targets, for a 2° amplitude yaw motion, period 3 s, towfish altitude 10 m.

The reduction in backscanning seen in the single-beam simulations as the period of the towfish motion increased, was repeated in the MBEAM simulations, and the remarks in Report I pertaining to this effect apply equally to the MBEAM model.

7. *Yaw Correction Modelling*

The Klein Multiscan and other multiple-beam sonars employ relatively slow refresh rates for their element weight and phase-delay settings, which may allow some adjustment for towfish orientation with sufficiently fast processing. Given that the most important towfish motion is likely to be yaw, it was of interest to determine whether a simple yaw correction could significantly improve the sidescan image.

It was assumed that the towfish contained some kind of orientation sensor, say a magnetic or gyroscopic compass, which would allow a determination of the towfish yaw orientation relative to the ideal tow path at the moment when each pulse was emitted. The yaw deviation would then be subtracted from the angles used by the beamformers, so that the beams would be re-directed directly across-track at the moment of pulse emission. As the echoes returned, the towfish would continue to move, and the success of the correction would depend on the amplitude of the subsequent motion.

An additional factor, which was not modelled in this work, is the effect of the additional steering on the reception beam patterns. As beams from a multiple-element beamformer with elements longer than a wavelength are steered away from broadside, sidelobe levels become progressively larger, until they are comparable to or exceed the size of the main lobe. For example, it is probable that the beams of the Klein Multiscan sonar are very seriously degraded by a 2° steering offset, since the individual transducer elements are 10 cm long and have beam nulls approximately 2° from broadside. A similar steering limitation is likely to apply to all multiple-beam sonars of similar construction.

The yaw correction was incorporated in the MBEAM model by an adjustment of the towfish orientation , rather than by individual beam resteering. Referring to Report I, the yaw orientation β was recorded at the moment of each pulse emission, and subtracted from all subsequent values of β during the calculations for echo receptions from that pulse. The time required for each simulation was only minimally affected by the yaw correction modelled in this way.

Simulations were performed for yaw motions of 1° and 2° amplitude with periods of 3 s including this simple correction, and the MBEAM images are shown in Figures 10 and 11 respectively. Comparing Figure 10 with Figure 8, the yaw correction has clear benefits, since the backscanning has been removed, along with most of the distortion and movement of the targets. Some parts of the image have faded, however, due to the mismatch between the beam footprints at emission (which cannot be steered in the MBEAM model) and reception.

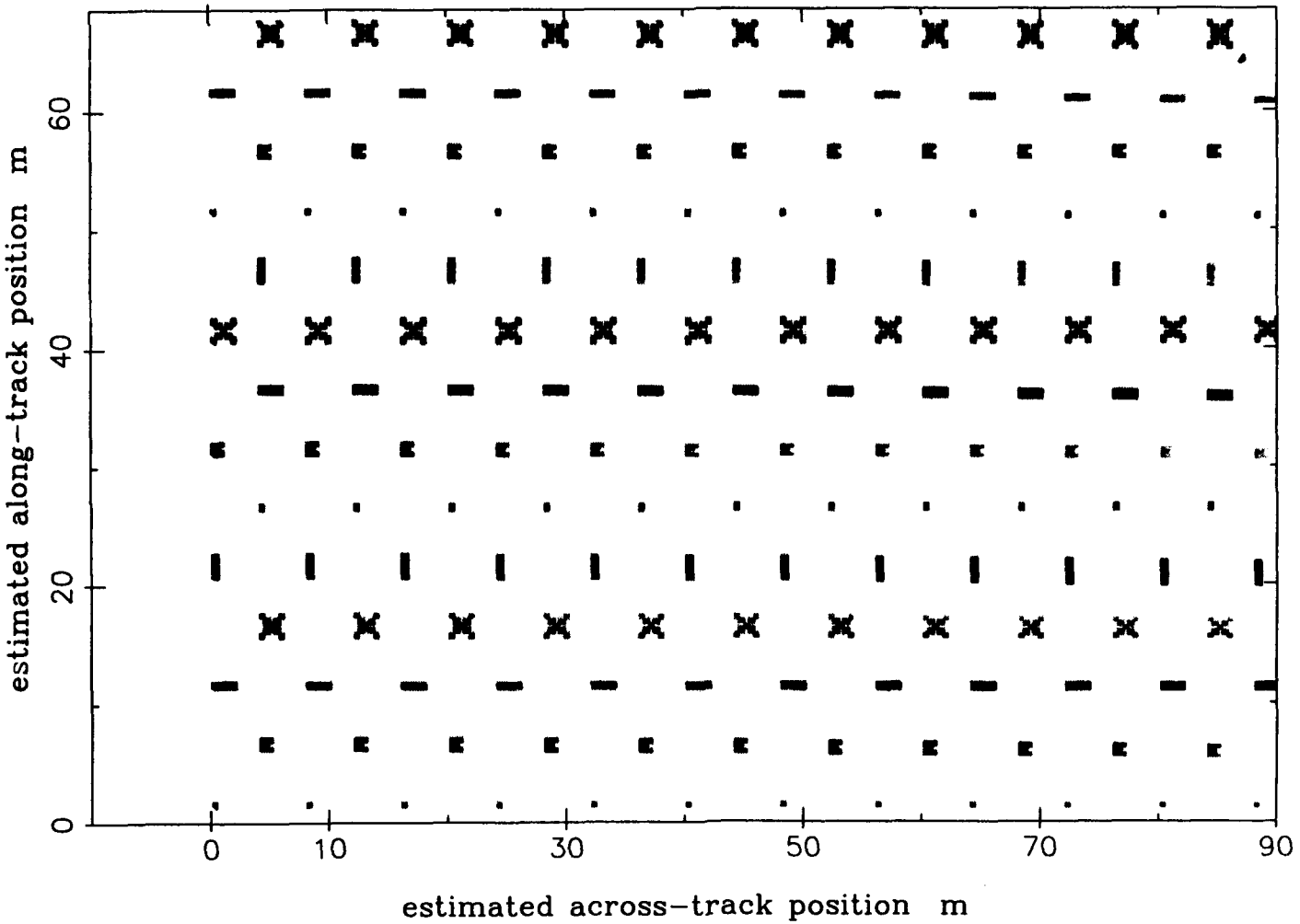

Figure 10: *Simulated MBEAM image of the targets, for a 1° amplitude yaw motion, period 3 s, towfish altitude 10 m, after yaw correction as described in section 7.*

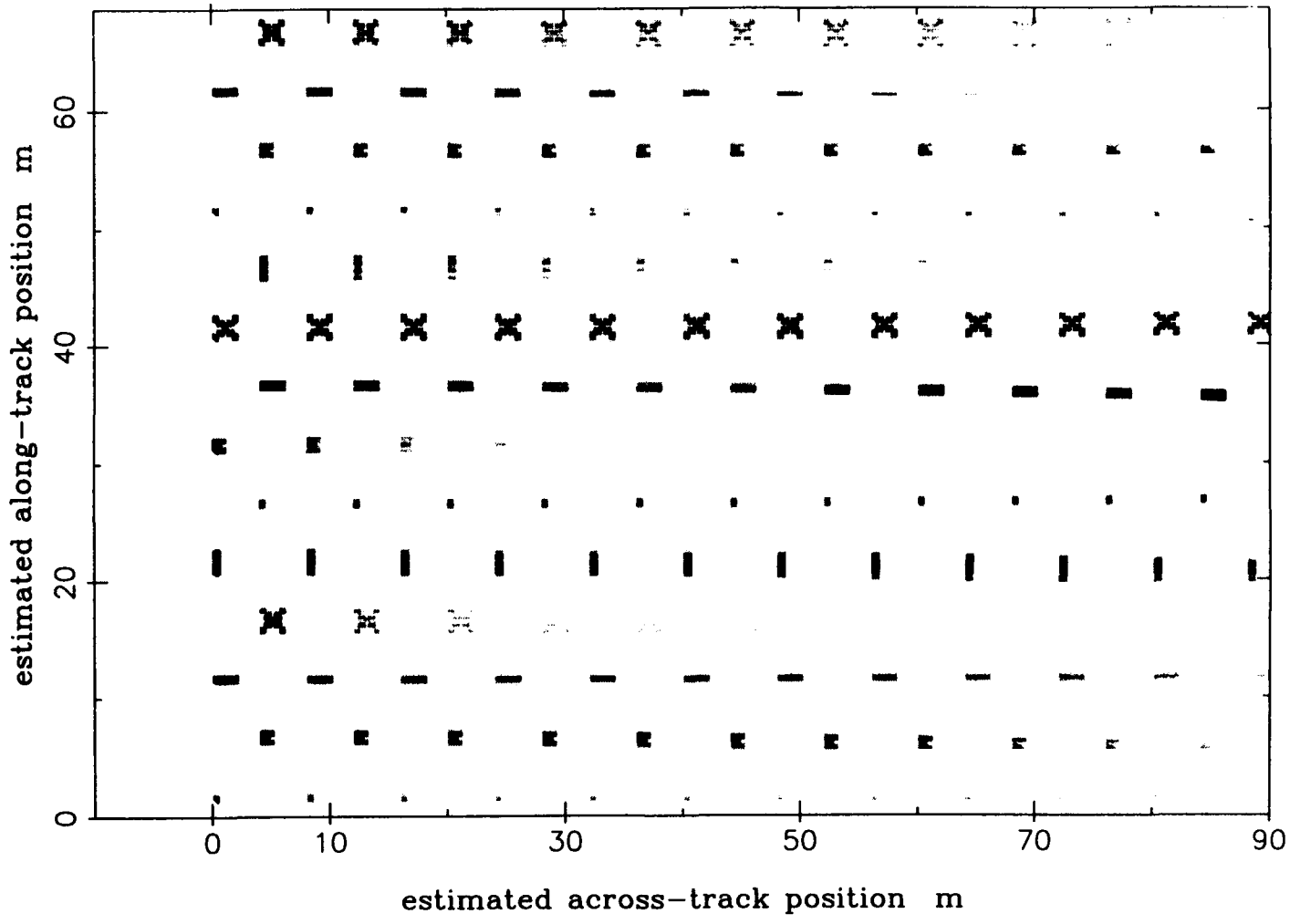

Figure 11: Simulated MBEAM image of the targets, for a 2° amplitude yaw motion, period 3 s, towfish altitude 10 m, after yaw correction as described in section 7.

Comparing Figure 11 with Figure 9, the benefit of yaw correction is much reduced, since fading has affected most of the image. In addition, not all of the backscanning and distortion has been removed, and as mentioned previously, a beam steering offset possibly as large as 2° may be impossible to obtain with available transducers. Without further modelling of the effects of beam steering, it can be concluded that yaw motion correction along the lines noted here would probably benefit images in conditions of up to 1° yaw.

Larger yaw amplitudes, even with much longer periods than 3 s, could probably not be corrected by redirection of the MBEAM sonar beams. However, it is likely that the degradation in coverage of the bottom caused by high *rates* of yaw could be remedied by a smaller adjustment of the reception beam steering direction, to direct the reception beam to the yaw orientation recorded at the moment that the pulse was emitted. Backscanning and object distortion would not be reduced to the same extent by such a correction as they would by the correction for absolute yaw orientation applied above. Further, because high rates of yaw are associated with small yaw angles and vice versa, it may be possible to devise hybrid algorithms which act to reduce extreme yaw angles with their associated distortion and backscanning, while improving bottom coverage.

8. *Conclusions*

This report has presented the results of simulations for a multiple-beam sidescan sonar model, MBEAM, based on the parameters noted for the Klein Associates Multiscan sonar, which show that thresholds for unacceptable towfish motions are approximately the same for the Multiscan as for a single-beam device operating at the same range-scale. It was however noted that the characters of the distortions are quite different. The operational consequences of this difference are not known and should be investigated experimentally.

Considering MBEAM images as a whole, where distortion of small objects is not important, the following maximum values for towfish motion are recommended, for a 3 s period:

(i) heave amplitude 1/10th the smallest important horizontal range;
(ii) sway amplitude 1 m;
(iii) roll was not simulated, but 10° amplitude is an estimate;
(iv) pitch amplitude of 6° at altitude 10 m, and equivalently surge amplitude of 1 m;
(v) yaw amplitude of 1°.

Where small objects, say a few beam-separations in size, are important, and even small levels of backscanning are intolerable, the following maximum values are recommended, with period 3 s:

(i) heave amplitude 1/40th the smallest important horizontal range;
(ii) sway amplitude 0.5 m;
(iii) roll was not simulated, but 10° amplitude is an estimate;
(iv) pitch amplitude of 3° at altitude 10 m, and equivalently surge amplitude of 0.5 m;
(v) yaw amplitude of 0.5°.

As was the case for a single-beam sidescan sonar, yaw is the motion with most potential to degrade the image of a multiple-beam device.

A simple yaw correction technique has been demonstrated, and found to be of benefit for yaw amplitudes of up to 1°. At higher yaw amplitudes, coverage and beam-steering problems make the technique less viable.

9. Acknowledgments

The author wishes to acknowledge the help of Dr Martin Lawrence via constructive criticism throughout the course of this work, and of this report, and the referee Dr Lynn Booth for helpful comments and corrections to the report.

10. References

Anstee, S. D., (1993) [Report I]
The effects of towfish motion on sidescan sonar images. MRL report in publication.

Fox, P. A., (1985)
An electronically focused multiple beam sidescan sonar. (PhD Thesis) Cape Town: University of Cape Town

Fox, P. A. and Denbigh, P. N., (1983)
An electronically focused multibeam sidescan sonar. *Proceedings of Acoustics and the Sea Bed Conference,* 347-355. Bath, UK: University of Bath

Huff, L. C., Langhorne, N., Quigley, R., Weintroub, J., Kuwahara, R., Preston, J. and Hart, A., (1991)
Multi-beam focused sonar (MBFS) experiments, Plymouth, UK, June-July 1991. MCM Specialist Group Report, The Technical Cooperation Program, Subgroup G.

Huff, L. C. and Weintroub, J., (1992)
Field measurements of a multibeam dynamically focused side scan sonar's along track resolution. *Proceedings of the 1992 U.S. Hydrographic Conference, Baltimore, Maryland.* 97-102

Huff, L. C., (1993)
High-resolution multi-beam focused side scan sonar. *Proceedings of the Institute of Acoustics,* 15, 2, 389-405.

SECURITY CLASSIFICATION OF THIS PAGE **UNCLASSIFIED**

REPORT NO.	AR NO.	REPORT SECURITY CLASSIFICATION
MRL-TN-660	AR-008-628	Unclassified

TITLE

The effects of towfish motion on sidescan sonar images: extension to a multiple-beam device

AUTHOR(S)
S.D. Anstee

CORPORATE AUTHOR
DSTO Materials Research Laboratory
PO Box 50
Ascot Vale Victoria 3032

REPORT DATE	TASK NO.	SPONSOR
February, 1994	NAV 91/165	MSPD

FILE NO.	REFERENCES	PAGES
510/207/0036	6	31

CLASSIFICATION/LIMITATION REVIEW DATE

CLASSIFICATION/RELEASE AUTHORITY
Chief, Maritime Operations Division MRL

SECONDARY DISTRIBUTION

Approved for public release

ANNOUNCEMENT

Announcement of this report is unlimited

KEYWORDS

MBEAM
Sonar Beams
Sidescan Sonar Images
Towfish Motion

ABSTRACT

A simulation algorithm previously used to estimate the geometrical effects of towfish motion on single-beam sidescan sonar images is modified to simulate a multiple-beam sidescan sonar. The parameters of the sidescan sonar model are based on those announced for the Multiscan sonar soon to be manufactured by Klein Associates Inc. The results of simulations using the algorithm are discussed and compared with previous results for a single-beam device. The thresholds for towfish motions producing unacceptable image distortion are found to be similar to those found for the single-beam device. The image distortions induced by the motions are however found to be qualitatively different from those seen with the single-beam sonar. The effects of and limitations to a simple yaw-correction scheme are also discussed.

The Effects of Towfish Motion on Sidescan Sonar Images: Extension to a Multiple-Beam Device

S.D. Anstee

(MRL-TN-660)

DISTRIBUTION LIST

Director, MRL - title page only
Chief, Maritime Operations Division
Dr B.F. Wild
Dr S.D. Anstee — 8 copies
MRL Information Services

Chief Defence Scientist (for CDS, FASSP, ASSCM) — 1 copy
Director (for Library), Aeronautical Research Laboratory
Head, Information Centre, Defence Intelligence Organisation
OIC Technical Reports Centre, Defence Central Library
Officer in Charge, Document Exchange Centre — 8 copies
Air Force Scientific Adviser, Russell Offices
Navy Scientific Adviser
Scientific Adviser - Policy and Command
DASD, APW2-1-OA2, Anzac Park West, Canberra ACT
Senior Librarian, Main Library DSTOS
Librarian - MRL Sydney — 5 copies
Librarian, DSD, Kingston ACT
Librarian, Australian Defence Force Academy
Serials Section (M List), Deakin University Library, Deakin University, Geelong 3217
NAPOC QWG Engineer NBCD c/- DENGRS-A, HQ Engineer Centre, Liverpool Military Area, NSW 2174
ABCA, Russell Offices, Canberra ACT 2600 — 4 copies
Head of Staff, British Defence Research and Supply Staff (Australia)
NASA Senior Scientific Representative in Australia
INSPEC: Acquisitions Section Institution of Electrical Engineers
Head Librarian, Australian Nuclear Science and Technology Organisation
Senior Librarian, Hargrave Library, Monash University
Library - Exchange Desk, National Institute of Standards and Technology, US
Acquisition Unit (DSC-EO/GO), British Library, Boston Spa, Wetherby Yorkshire LS23 7BQ, England
Library, Chemical Abstracts Reference Service
Engineering Societies Library, US
Documents Librarian, The Center for Research Libraries, US
Library, Deakin University
Army Scientific Adviser, Russell Offices - data sheet only
Director General Force Development (Land) - data sheet only
SO (Science), HQ 1 Division, Milpo, Enoggera, Qld 4057 - data sheet only
Counsellor, Defence Science, Embassy of Australia - data sheet only
Counsellor, Defence Science, Australian High Commission - data sheet only
Scientific Adviser to DSTC Malaysia, c/- Defence Adviser - data sheet only
Scientific Adviser to MRDC Thailand, c/- Defence Attache - data sheet only

Research Leader, Submarine and Ship Sonar, MOD
Research Leader, Mine Warfare Operations, MOD
Mine Sweeping Project Director, DP2-3-06, Campbell Park Offices, Canberra ACT 2600
L. Booth, MOD Sydney
K.E. Gross, MOD Sydney
M.W. Lawrence, MOD Sydney
G. Campanella, MOD Melbourne
R.A. Neill, MOD Melbourne
P.C. Pamias, MOD Melbourne

(MRL-TN-660)

DISTRIBUTION LIST
(Continued)

Commander Australian Minewarfare Forces, HMAS Waterhen, Waverton NSW
Deputy Director Mine Warfare Development, B-4-01, Russell Offices, Canberra ACT
Director Minor Project Development, MHQ, Potts Point NSW
Mine Warfare Systems Centre Project Director, CP2-2-19, Campbell Park Offices, Canberra ACT
OIC, Mine Warfare Operational Support Section, HMAS Waterhen, Waverton NSW
Mine Warfare Operations Officer, HMAS Waterhen, Waverton NSW
Mine Warfare Route Survey Officer, HMAS Waterhen, Waverton NSW